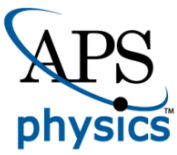

Variation of sign and magnitude of the Dzyaloshinskii-Moriya interaction of a ferromagnet with an oxide interface

Monika Arora, Justin M. Shaw, and Hans T. Nembach

Phys. Rev. B **101**, 054421 — Published 18 February 2020

DOI: 10.1103/PhysRevB.101.054421

Variation of sign and magnitude of the Dzyaloshinkskii-Moriya interaction of a ferromagnet with an oxide interface

Monika Arora[1,2], Justin M. Shaw[1] and Hans T. Nembach[1,3]

[1]National Institute of Standards and Technology, Boulder, CO 80305, USA

[2]Department of Physics, University of Colorado, Boulder, CO 80309, USA

[3]JILA, University of Colorado, Boulder, CO 80309, USA

We demonstrate that both the magnitude and sign of the Dzyaloshinskii-Moriya interaction can be tuned by modifying the type and thickness of an oxide layer adjacent to a ferromagnet. We focus on Ti/Cu/$Co_{90}Fe_{10}$/Ta(d_{Ta})/Oxide/Ta structures, where the Ta interlayer thickness d_{Ta} ranged from 0 nm to 3 nm, followed by an exposure to oxygen and "Oxide" can mean $CoFeO_x$ and/or TaO_x. We used Brillouin light scattering spectroscopy to directly determine the volume-averaged Dzyaloshinkii-Moriya interaction from the non-reciprocity of the spin-wave frequency. The magnitude of the interfacial Dzyaloshinkskii-Moriya interaction, D_{DMI}, ranges from – 0.17 to + 0.09 (± 0.02) mJ/m^2, clearly showing a change in both sign and magnitude, with an increase of Ta interlayer thickness. The modification of the oxide interface allows us to systematically change the hybridization of the 3*d*-CoFe orbitals from 3*d*-5*d* to 3*d*-2*p* and analyze the influence on the Dzyaloshinskii-Moriya interaction. Importantly, we can vary the Dzyaloshinskii-Moriya interaction while maintaining a relatively small value of the damping parameter.

INTRODUCTION

It has been recognized that the Dzyaloshinskii-Moriya interaction (DMI) can promote chiral spin texture phases such as magnetic skyrmion lattices, chiral spin chain, and domain walls in ferromagnetic materials [1-3]. Spin textures with a fixed chirality are both fundamentally interesting and technologically promising due to their potential applications in ultra-high-density data and memory technologies [1].

Fundamentally, DMI is an anti-symmetric exchange interaction, which favors non-collinear alignment of neighboring spins S_i and S_j, in contrast to the Heisenberg or symmetric exchange interaction, which stabilizes a collinear magnetization. There are two types of DMI: bulk and interfacial DMIs. The bulk DMI arises as a result of lack of inversion symmetry in the crystal structures typically observed in oxides such as Fe_2O_3 (Hematite) and B20 compounds such as MnSi [2-4]. However, the interfacial DMI generally originates from the interface between a ferromagnet (FM) and a heavy metal (HM) [2,3]. In such systems, interfacial DMI is mediated by an atom in the high spin-orbit material, which ultimately favors canting of neighboring spins that can lead to chiral spin textures [2,3,5]. Spin spirals and magnetic skyrmions in ultra-thin films were first observed in Mn/W(110) [6] and that later in Mn/W(100), Cr/W, Fe/Ir and PdFe/Ir systems [7-11]. It is found that the total free energy and magnetic order in the Mn films strongly depends on the crystallographic planes of the W(110) and W(100) substrates [6-7].

Recent experiments have demonstrated that thin FM layers with perpendicular magnetic anisotropy (PMA) and sufficiently large DMI favor Néel over Bloch walls with a fixed chirality. The combination of such chiral domain wall structures with spin-orbit torque enables fast current induced domain wall motion [12], where the chirality and speed of the domain wall depend on the sign and magnitude of spin-orbit torque and the magnitude of DMI [2, 13]. Therefore, understanding how to control the sign and magnitude of DMI is needed to design the next generation magnetic memory based on chiral magnetic domain walls and skyrmions.

To date, most of the experimental work on interfacial DMI [14] has been confined to heavy metals/ferromagnet interface, where heavy metals such as Pt, Ir and W are used to induce DMI. The use of these metals is also known to enhance the damping parameter α due to spin memory loss and spin pumping [15-16]. It has been shown that the domain wall mobility, which varies as $1/\alpha^2$, can be drastically increased for small damping values [17]. Also, large damping results in low energy efficiency. Therefore, maintaining low damping is crucial for the operating speed of devices based on domain wall motion driven by spin-orbit torque. Oxide interfaces show significantly reduced spin pumping contribution to the damping and are therefore a potential alternative to heavy metals.

Recent density functional theory (DFT) calculations performed by Belabbes et al. [18] predict that the magnitude and sign of DMI can be controlled by changing the oxygen coverage of the FM layer. The calculations show a correlation between DMI and an electric dipole moment at the FM/oxide interface, where the electric dipole moment is a result of the hybridization of the 3*d*-orbitals of the ferromagnet and the *p*-orbitals of oxygen together with the associated charge transfer. A similar study demonstrates more generally that the DMI can be tuned by an electric field, which results in a charge transfer at the interface [19, 20]. Recently, the existence of DMI at the CoFe/Oxide interface has been demonstrated [21].

In this work, we show that both the magnitude and sign of DMI can be tuned by varying the type and/or thickness of an oxide layer adjacent to a ferromagnetic film, which changes the electronic structure at the interface. We fabricated a series of sputtered multilayer stacks consisting of substrate/Ti(3)/Cu(5)/$Co_{90}Fe_{10}$(1.5)/Ta(d_{Ta})/Oxide/Ta(3) structures, (thicknesses in nanometers), where "Oxide" can mean $CoFeO_x$ and/or TaO_x. The thickness of Ta(d_{Ta}) is systematically varied to change the nature of the oxide in contact with the $Co_{90}Fe_{10}$ (hereafter referred to as CoFe). Since it is not straightforward to separate the DMI contributions originating from the top and bottom FM interfaces, the Cu seed layer structure is kept constant for all samples, so that variation in the DMI can be ascribed to the top interface between the CoFe and the oxide layer. We show that the type and thickness of the oxide layer also affects the magnetic anisotropy, magnetic moment, and magnetic damping. Understanding how oxides affect DMI at interfaces will provide an efficient way to control the DMI.

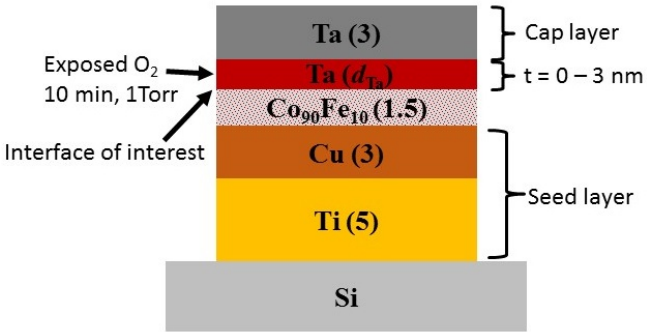

Figure 1: Schematic representation of the full film structure, Ti(5)/Cu(3)/$Co_{90}Fe_{10}$ (1.5)/Ta(d_{Ta})/Ta(3) where the thickness of Ta(d_{Ta}) is varied from 0 to 3 nm (thicknesses in nanometers) followed by an exposure to oxygen. The Ti and Cu layers are seed layers and the top Ta layer is a capping layer.

EXPERIMENTAL DETAILS

A series of samples (as shown in Figure 1) was deposited by magnetron sputtering on thermally oxidized Si (100). The Ti layer serves as an adhesion layer as well as promoting a (111) texture in Cu, and ultimately, in CoFe. Following deposition of the Ta(d_{Ta}) layer, samples were transferred to the load-lock chamber where they were exposed to oxygen at a pressure of 1.3×10^2 Pa (1 Torr) for 10 minutes, to form an oxide layer. By varying the thickness d_{Ta} of the Ta layer deposited prior to the oxidation, we systematically vary the type/thickness of the oxide at the interface of CoFe. Following the oxidation step, the load-lock was pumped down before the samples were transferred back to the main deposition chamber. After the main chamber pressure reached approximately 3×10^{-7} Pa (2×10^{-9} Torr), a final capping layer of 3 nm Ta was deposited on top of the oxide layer to prevent any further oxidation. In addition to the samples described above, we prepared a control sample substrate/Ti(5)/ Cu(3)/ CoFe(1.5)/Ta(3), without any oxidation layer. During the growth process, the substrate temperature was kept constant at room temperature. All deposition rates were calibrated using x-ray reflectivity measurements.

The magnetic moment was measured with a commercial superconducting quantum interference device (SQUID) magnetometer. Measurements were performed in magnetic fields of up to $\mu_0 H$=2 T, with the field applied parallel to the sample surface. We measured hysteresis curves of 6×6 mm chip to obtain the saturation magnetization M_s(300K). The thickness of the dead layer is calculated by using the equation $M_s = m/A \cdot d$, where m is the measured magnetic moment, A and d are respectively the area and magnetic thickness of the film. We used a 14 nm thick film of CoFe to calculate the M_s. The dead layer is calculated from the difference between the physical thickness (determined from x-ray reflectometry calibration of deposition rates) and magnetic thickness (determined from SQUID magnetometry). We determined the symmetric exchange A_{ex} by fitting the low temperature magnetic moment-temperature (m-T) curve to Bloch's $T^{3/2}$ law as described in [22, 23].

We performed broadband ferromagnetic resonance (FMR) spectroscopy with a room-temperature bore superconducting magnet capable of applying magnetic fields up to $\mu_0 H$=3 T. Samples were first coated with poly (methyl methacrylate) (PMMA) to provide

both mechanical protection and to prevent direct electrical contact to the co-planer waveguide (CPW). Samples were then placed face-down on a CPW with a nominal impedance of 50 Ω. The CPW was connected to a vector network analyzer (VNA) with a 70 GHz bandwidth and the complex S_{21} transmission parameter (ratio of the voltage applied at one end of the CPW to the voltage measured at the other end) was measured over a wide range of frequencies as the external magnetic field was swept through the FMR resonance as described in Refs. [24-26]. The perpendicular anisotropy field H_k and the spectroscopic splitting factor g for the out-of-plane geometry were determined from the fits to the Kittel equation:

$$f = \frac{\mu_0 \mu_B g}{h}\left(H - M_{eff}\right), \quad (1)$$

where $M_{eff} = M_s - H_k$ is the effective magnetization, H is the applied magnetic field, h is the Planck constant, μ_0 is the vacuum permeability and μ_B is the Bohr magneton. The damping parameter α was determined from a fit to the equation:

$$\Delta H = \frac{2h\alpha}{g\mu_0 \mu_B} f + \Delta H_0 \quad (2)$$

where ΔH is FMR linewidth, α is the total damping, which includes contributions from spin-pumping and spin-memory loss in addition to the intrinsic damping. ΔH_0 is the inhomogeneous linewidth.

We used a Brillouin light scattering spectrometer (BLS) with a six-pass, tandem Fabry-Perot interferometer to measure the frequency of thermal spin waves at a fixed angle of incidence θ = 45°. A 532 nm laser beam was focused onto a sample, and thus the wavevector of the measured spin waves was k = 16.7 μm^{-1}. The measurements were performed in the Damon-Eshbach (DE) geometry, where the magnetic field is applied perpendicular to the plane of incidence and the DE spin wave modes propagate perpendicular to the direction of the magnetic field. Interfacial DMI will induce an asymmetric spin-wave dispersion (i.e., spin waves propagating in opposite directions will have different frequencies). The frequency of the spin waves is given by

$$f_M(k) = f_0 + \Delta f_{DMI}(k) \quad (3)$$

where f_0 is the frequency of the spin waves in the absence of DMI and Δf_{DMI} is the shift of the spin wave frequency due to the presence of the DMI.

We determined the frequency for the Stokes and anti-Stokes peak for both field polarities, which in turn allowed us to determine the magnitude and sign of the volume averaged DMI, D_{DMI} using

$$\Delta f_{\mathrm{DMI}} = \left|\frac{g^{||}\mu_{\mathrm{B}}}{h}\right| sgn(M_{\mathrm{z}})\frac{2D_{\mathrm{DMI}}}{M_{\mathrm{S}}}.k \qquad (4)$$

where, $g^{||}$ is the in-plane spectroscopic splitting factor.

The interfacial DMI, $D_{\mathrm{DMI}}^{\mathrm{int}}$, can be calculated as

$$D_{\mathrm{DMI}}^{\mathrm{int}} = D_{\mathrm{DMI}}.t, \qquad (5)$$

where t is the magnetic thickness of the CoFe layer.

RESULTS AND DISCUSSION

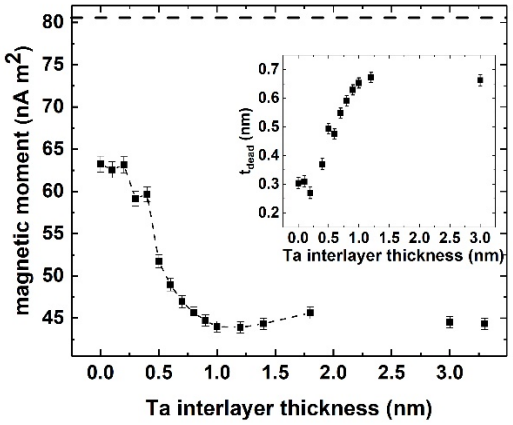

Figure 2: Measured magnetic moment of CoFe as a function of Ta interlayer thickness d_{Ta} measured at 300K (dashed line as a guide to the eye). The inset is a plot of the calculated dead layer of CoFe. (The magnetic dead layer thickness is determined from comparison of the magnetic moment of each sample to the magnetic moment of a 14 nm thick CoFe sample measured at 10 K. The horizontal dotted line indicates the ideal value of magnetic moment assuming M_s = (1.882 ± 0.009) T at 10 K.

Figure 2 shows the measured magnetic moment samples at 300 K of the relevant samples as a function of Ta interlayer thickness d_{Ta}. The magnetic moment initially decreases for d_{Ta} up to approximately 1 nm. Above 1 nm, the magnetic moment stays approximately constant within the scatter of the data. The trend in the magnetic moment

can be explained by taking into account the formation of an "Oxide" layer at the CoFe/Ta interface, in combination with intermixing/diffusion of Ta into CoFe (The modification of CoFe interfaces due to oxidation is discussed later. See sample stacks in Figure 4). The decrease of the magnetic moment due to the formation of a dead layer at a FM/Ta interface due to intermixing of the FM with Ta is commonly observed [27-29].

The dead layer thickness can be determined by calculating the deviation of the measured magnetic moment for each sample from the expected value based on the bulk M_s and the nominal thickness. We used M_s (T=10 K) = (1.882 ± 0.009) T of a 14 nm thick CoFe film measured as a bulk value and the respective magnetic moment measured at T= 10 K to determine the dead layer thickness of each sample (shown as an inset of Figure 2). Even though we assume a fixed value for M_s at 10 K for all samples, the room temperature values for M_s can be different for each sample due to their respective exchange interaction.

It is interesting to note that exposing the bare CoFe to oxygen only consumes about 1.5 monolayers (~0.3 nm) of CoFe, but as more Ta is deposited, the dead layer continues to increase until at about Ta (d_{Ta}) = 1 nm where it saturates at approximately 0.7 nm. This value is consistent with the previously reported values [27-29] of estimated dead layer thicknesses ranging from 0.25 nm to 0.6 nm at the FM/Ta interfaces.

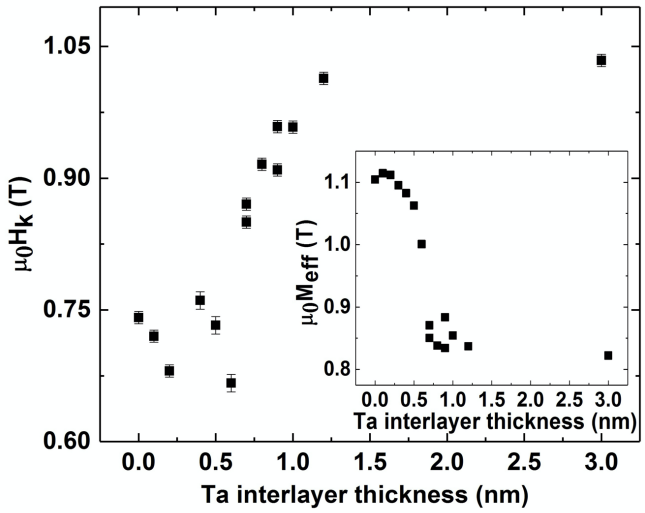

Figure 3: Plot of the perpendicular anisotropy field $\mu_0 H_k = \mu_0 M_{eff} - \mu_0 M_s$ as a function of Ta interlayer thickness d_{Ta}, where M_s is calculated from the measured magnetic moment at 300 K by taking into account the thickness of dead layer of each sample (shown earlier as an inset of Figure 2). The inset shows a plot of effective magnetization $M_{eff.}$ determined from FMR data.

Figure 3 shows the variation of interfacial perpendicular anisotropy $\mu_0 H_k = \mu_0 M_{eff} - \mu_0 M_s$ as a function of the Ta interlayer thickness d_{Ta}, where M_{eff} is the effective magnetization determined from FMR data using Eq. (1) and M_s is determined from the measured magnetic moment at 300 K under consideration of the dead layer. The anisotropy $\mu_0 H_k$ shows a gradual increase with increase in Ta interlayer thickness, until it saturates at above 1 nm. Our results agree with those found in the literature [30-32], where a similar trend of increase in perpendicular anisotropy with the increase in degree of oxidation has been reported for Co (Fe) /MO_x interfaces (M = Ta, Mg, Al, Ru etc.). It is demonstrated that despite the weak spin orbit interaction (SOI) at the Co (Fe) /MO_x interfaces, the hybridization between the Co (Fe)-3*d* and O-2*p* orbitals can give rise to PMA even stronger than that of Co/Pt interfaces (high SOI) [33]. Furthermore, the largest PMA is observed for interfaces with the optimum oxygen coverage, while it is reduced for over or under oxidized interfaces [30, 33-34].

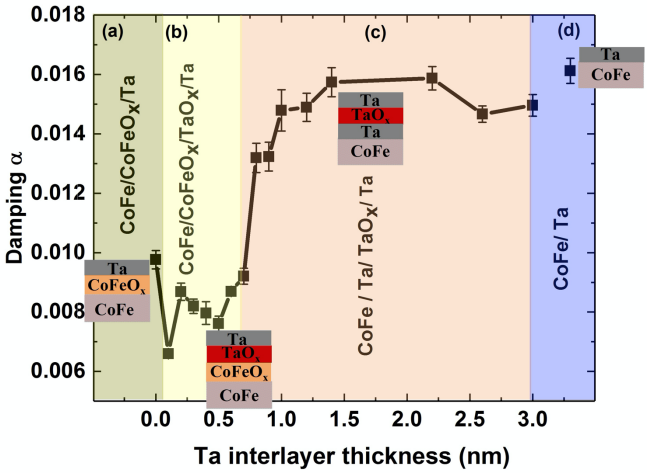

Figure 4: Dependence of damping α of Ti(5)/Cu(3)/CoFe(1.5)/Ta(d_{Ta})/Oxide/Ta(3) as a function of Ta interlayer thickness, where d_{Ta} ranges from 0 to 3 nm. FMR measurements were performed at room temperature. The sample stack shown in the plot illustrate the change of the interfaces with increasing Ta interlayer thickness, d_{Ta}.

From the frequency dependence of the linewidth [Eq. (2)], we determine the damping constants of our samples, which is plotted in Figure 4. It is foremost to mention here that the damping values are relatively small in comparison to the heterostructures with comparable FM/HM interfaces with a damping value of 0.02 [16, 35]. The damping

constant α remains unchanged, albeit scattered, for samples with $d_{Ta} < 0.7$ nm. Above 0.7 nm, a significant increase in α is observed until a thickness of approximately 1.0 nm, after which the damping values saturate. This data provides strong evidence about the nature of the interface that is exposed to oxygen. For the case of a CoFe/oxide interface, spin-pumping at the CoFe/oxide interface is expected to be strongly suppressed [36-39]. However, at a CoFe/Ta interface, an enhancement of the damping is expected from spin pumping losses into the metallic Ta layer or spin memory losses at the interface [15]. In addition, Ta is known to have an exceptionally small spin diffusion length (< 1 nm) [40]. As a result, the data in Figure. 4 suggests that a CoFe/oxide interface is present from 0 nm $\leq d_{Ta} \leq 0.7$ nm and metallic Ta begins to form at the interface of the ferromagnet above d_{Ta} = 0.7 nm, indicated by the dramatic increase in the damping parameter. Since the spin diffusion length of Ta is less than 1 nm, it would be expected that the enhanced damping due to spin-pumping would saturate within 1 nm of Ta. Indeed, this is consistent with our experimental observation.

Based on these arguments, we identify four regions in Figure 4 as a guide to the structure formation at the top interface of CoFe as a function of Ta interlayer thickness d_{Ta}. Region (a) refers to $CoFeO_x$/Ta interface as there is no Ta present during the oxidation (d_{Ta} = 0 nm). With the addition of Ta interlayer, we expect a mix of $CoFeO_x$ and TaO_x at the interface adjacent to CoFe. A further increase of d_{Ta} increases the fraction of TaO_x until it starts to form metallic Ta (schematic representation of the interface structure is shown in Figure 4). Since the damping stays nearly constant for a Ta thickness below 0.7 nm, we identify region (b) ($0.1 \lesssim d_{Ta} \lesssim 0.7$ nm) as structures with CoFe/Oxide interfaces. Region (c) is assigned to Ta interlayer thicknesses for which we see an abrupt increase in damping parameter until it saturates at above 1 nm, clearly indicating the CoFe/Ta nature of the interface. In addition, a saturation of the perpendicular anisotropy and a levelling off of the dead layer thickness (although not as sharp and dramatic) in the same approximate range of d_{Ta} is probably due to having metallic Ta adjacent to CoFe. Region (d) highlights the structure of the control sample with CoFe/Ta interface. We observed that the magnetic data (Figures 2-4) for Ta interlayer thicknesses above 1 nm (region (c)) have a proximity to the

data of the control sample (region (d)), presenting a strong evidence of a CoFe/Ta interface in region (c).

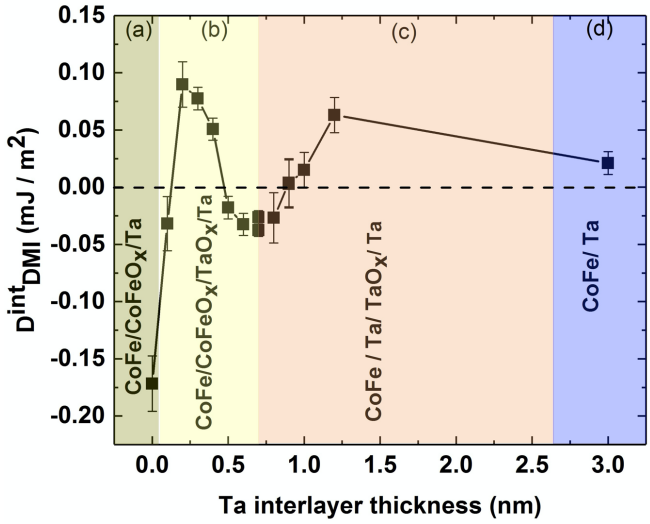

Figure 5: Plot of interfacial D^{int}_{DMI} in Ti(3)/Cu(5)/CoFe(1.5)/Ta(d_{Ta})/Ta(3) as a function of Ta interlayer thickness. Brillouin light scattering is used to measure the DMI induced frequency shift in the samples that is subsequently used to calculate D^{int}_{DMI} with Eq (4) and (5).

Figure 5 shows a plot of interfacial DMI $D^{\mathrm{int}}_{\mathrm{DMI}}$ that was determined from the frequency shift measured by BLS using Eqs. (4) and (5). The error bars are determined from the experimental uncertainties of Δf_{DMI}, M_s and $g^{\perp}$. Here, we are using $g^{\perp}$ due to the large error bars in $g^{\parallel}$, which was obtained from in-plane FMR measurements Note that, we are using a sign convention for the DMI, where a negative (positive) sign corresponds to left-handed (right-handed) chirality. D^{int}_{DMI} is very small and positive for the control sample [region (d)]. The small value of $D^{\mathrm{int}}_{\mathrm{DMI}}$, is in accordance with the fact the interfacial DMI is usually small for early 5*d* elements like Hf and Ta due to their small SOC [41]. $D^{\mathrm{int}}_{\mathrm{DMI}}$, increases, accompanied by a sign reversal after oxidizing the CoFe surface [region (a) and (b)]. We furthermore observed a minimum in $D^{\mathrm{int}}_{\mathrm{DMI}}$, at the transition from region (b) to (c) until it stabilizes at above $d_{\mathrm{Ta}} = 1$ nm.

According to the DFT calculations performed by Belabbes et al. [18, 42], the magnitude and sign of DMI are related to (i) the oxygen coverage of the magnetic film [18], and (ii) the 3*d* orbital occupation and spin flip/mixing processes with the spin-orbit

active 5*d* states [42]. In addition, the magnetic chirality depends on the interplay between SOC, Hund's first rule, and the crystal field splitting of the *d* orbitals.

In our case, we assume that both effects play an important role in determining the D_{DMI}^{int} as a function of Ta interlayer thickness. For region (a) and (b), the variation in both the magnitude and sign of the $D_{\mathrm{DMI}}^{\mathrm{int}}$ value can be attributed to the varying thickness and composition of the "Oxide" adjacent to CoFe. Due to the oxidation process, CoFe-3*d* and O-2*p* orbitals hybridize, which is associated with a charge transfer from the FM layer to the oxygen atoms [43, 44]. Indeed, the variation in thickness of Ta interlayer from 0.1 nm to 0.7 nm modifies the degree of oxygen at the CoFe interface, thereby affecting the hybridization between 3*d*-2*p* orbitals and consequently the DMI.

In region (c) and (d), variation of DMI can be ascribed to the change in thickness of metallic Ta interlayer. The symmetry breaking at the CoFe/Ta interface and SOC gives rise to DMI. The increase in thickness of metallic Ta presumably influences the spin flip/mixing processes of 3*d* orbitals with the 5*d* states, resulting in change of DMI. The DMI increases with the Ta layer thickness below its spin diffusion length (~ 1 nm) and saturates above its spin diffusion length. The trend of increase in DMI at above 0.7 nm of d_{Ta} agrees with the findings by Tacchi et al. [45] and Avinash et al. [46] in their respective studies of Pt/CoFeB and Ta/CoFeB films.

The data clearly shows that both the magnitude and sign of interfacial DMI can be controlled by an oxide interlayer, which further depends on the thickness/type of oxidation. It is therefore, important to mention here that a Ta or oxide layer such as MgO and AlO_x, which are commonly used as an inert capping layer to protect the heterostructures, can contribute to the total DMI. Thus, the occurrence of DMI due to such oxide cap layer should not be ignored. Another importance finding of the study is that we were able to vary the DMI while maintaining a low damping parameter.

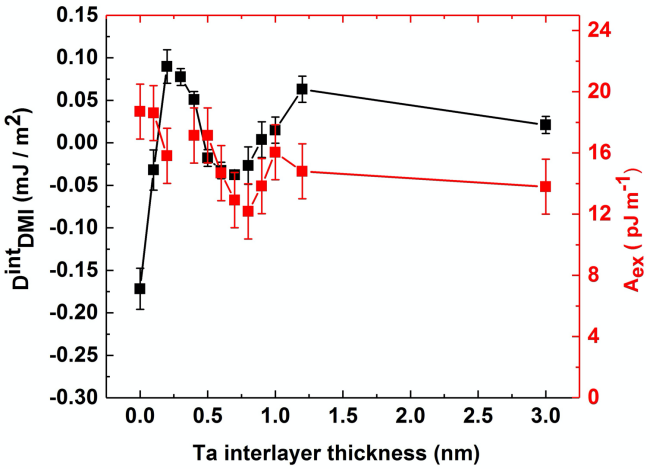

Figure 6: Plot of $D^{\text{int}}_{\text{DMI}}$ (left axis) and exchange constant A_{ex} (right axis) as a function of Ta interlayer thickness. The $D^{\text{int}}_{\text{DMI}}$ and A_{ex} data is presented by black squares and red empty squares respectively.

In order to examine the potential correlation of Heisenberg symmetric exchange A_{ex} and antisymmetric exchange DMI, we determined A_{ex} by fitting the low temperature magnetometry data of each sample to the Bloch $T^{3/2}$ law [22, 23]. In figure 6, we plot the D^{int}_{DMI} (left axis) and A_{ex} (right axis) as a function of Ta interlayer thickness. Although we do not observe a significant variation in the value of A_{ex} relative to the variation in D^{int}_{DMI}, both the symmetric A_{ex} and antisymmetric exchange D^{int}_{DMI} show some similar features with the variation of Ta interlayer thickness. For example, the values of both A_{ex} and $D^{\text{int}}_{\text{DMI}}$ show a decrease after 0.5 nm, obtain a minimum and continue to increase until 1 nm thickness of Ta interlayer. Although the A_{ex} and $D^{\text{int}}_{\text{DMI}}$ do not exhibit a strict resemblance over the entire dataset, the presence of many similar features in both A_{ex} and $D^{\text{int}}_{\text{DMI}}$ is consistent with the theory originally proposed by Moriya, whereby the DMI and Heisenberg exchange share the same underlying physics [47]. In some systems, this can manifest into a direct, linear relationship between the symmetric and antisymmetric exchange in NiFe films as was reported by Nembach et al. [22].

CONCLUSION:

In summary, we demonstrate that both the magnitude and sign of DMI can be controlled by changing the hybridization at the interface through modification of the oxygen exposure at the top interface of a ferromagnet. Our study is based on two different DFT calculations performed by Belabbes et al. [18, 42]. According to their first

calculations, the magnitude and sign of DMI can be entirely controlled by tuning the degree of oxidation of the magnetic film and the associated 3*d*-2*p* hybridization [42]. The second calculation focusses on DMI at metallic 3*d*-5*d* interfaces [18], where the DMI is directly correlated to the 3*d* orbital occupation and the spin flip/mixing processes with the spin-orbit active 5*d* states. In our experiment we systematically increased the thickness of the Ta layer adjacent to the ferromagnet prior to the in-situ oxidation until a metallic interface forms.

For a Ta thickness ranging from 0 to 0.7 nm, the DMI originates from the CoFe/Oxide interface, where Oxide can mean $CoFeO_x$ or TaO_x. The increase in thickness of Ta, which implies thicker TaO_x, varies the degree of oxidation at CoFe interface that affects the hybridization of 3*d*-CoFe and 2*p*-O orbitals together with the charge transfer and consequently DMI. However, for Ta thickness above 0.7 nm, the DMI arises due to the symmetry breaking and mixing of the 3*d*- and 5*d*- wavefunctions at the 3*d*-CoFe and the 5*d*-Ta interface together with the spin-orbit coupling of the Ta.

ACKNOWLEDGEMENT

This research was supported by DARPA award No. R18-687-0004 and DOE award No. DE-SC0017643. We are thankful to Grant Riley for helping in the calculation of exchange coupling and dead layer determination.

REFERENCES:

1. A. Fert, N. Reyren and V. Cros, Magnetic skyrmions: advances in physics and potential applications, Nature Reviews Materials. 2 17031 (2017).
2. I. E. Dzyaloshinskii, A thermodynamic theory of "weak" ferromagnetism of antiferromagnets, J. Phys. Chem. Solids. 4, 241-255 (1958).
3. T. Moriya, New mechanism of anisotropic super-exchange interaction, Physical Review Letters. 4, Number 5 (1960).
4. S. Muhlbauer, B. Binz, F. Jonietz, C. Pfleiderer, A. Rosch, A. Neubauer, R. Georgii and P. Boni, Skyrmion Lattice in a Chiral Magnet, Science 323, Issue 5916 (2009).

5. X. Z. Yu, Y. Onose, N. Kanazawa, J. H. Park, J. H. Han, Y. Matsui, N. Nagaosa and Y. Tokura, Real-space observation of a two-dimensional skyrmion crystal. Nature 465, 901 (2010).
6. M. Bode, M. Heide, K. von Bergmann, P. Ferriani, S. Heinze, G. Bihlmayer, A. Kubetzka, O. Piezsch, S. Blugal and R. Weisendanger, Chiral magnetic order at surfaces driven by inversion asymmetry, Nature 447, 190 (2007).
7. P. Ferriani, K. von Bergmann, E. Y. Vedmedenko, S. Heinze, M. Bode, M. Heide, G. Bihlmayer, S. Blugel, and R. Wiesendanger, Atomic-Scale Spin Spiral with a Unique Rotational Sense: Mn Monolayer on W(001). Phys. Rev. Lett. 101, 027201 (2008).
8. B. Santos, J. M. Puerta, J. I. Cerda, R. Stumpf, K. von Bergmann, R. Wiesendanger, M. Bode, K. F. McCarty and J. de la Figuera, Structure and magnetism of ultra-thin chromium layers on W(110). New J. Phys. 10, 013005 (2008).
9. B. Zimmermann, M. Heide, G. Bihlmayer and S. Blügel, First-principles analysis of a homochiral cycloidal magnetic structure in a monolayer Cr on W(110). Phys. Rev. B 90, 115427 (2014).
10. S. Heinze1, K. von Bergmann, M. Menzel, J. Brede, A. Kubetzka, R. Wiesendanger, G. Bihlmayer and S. Blügel, Spontaneous atomic-scale magnetic skyrmion lattice in two dimensions, Nat. Phys. 7, 713 (2011).
11. N. Romming, C. Hanneken, M. Menzel, J. E. Bickel, B. Wolter, K. von Bergmann, R. Wiesendanger, Writing and Deleting Single Magnetic Skyrmions, Science, 341(6146), 636–639 (2013).
12. I. M. Miron, T. A. Moore, H. Szambolics, L. D. Buda-Prejbeanu, S. Auffret, B. Rodmacq, S. Pizzini, J. Vogel, M. F. Jr Bonfim, A. Schuhl and G. Gaudin, Fast current induced domain wall motion controlled by the Rashba effect, Nat. Mater, 10, 419-423 (2011).
13. S. Emori, U. Bauer, S. M. Ahn, E. Martinez and G. S. D. Beach, Current-driven dynamics of chiral ferromagnetic domain walls, Nat. Mater, 12, 611–616 (2013).
14. S. Husain, N. Sisodia, A. K. Chaurasiya, A. Kumar, J. P. Singh, B. S. Yadav, S. Akansel, K. H. Chae, A. Barman, P. K. Muduli, P. Svedlindh and S. Chaudhary, Observation of Skyrmions at Room Temperature in Co_2FeAl Heusler Alloy Ultrathin Film Heterostructures, Scientific Reports volume 9, 1085 (2019).

15. A. Kumar, R. Gupta, S. Husain, N. Behera, S. Hait, S. Chaudhary, R. Brucas and P. Svedlindh, Spin pumping and spin torque in interfacial tailored Co2FeAl/β-Ta layers, arXiv:1904.01506 [cond-mat.mtrl-sci].
16. L. Zhu, D. C. Ralph, and R. A. Buhrman, Spin-orbit torques in heavy metal/ferromagnet bilayers with varying strength of interfacial spin-orbit coupling, Physical Review Letters 122, 077201 (2019).
17. R. Wieser, U. Nowak, and K. D. Usadel, Domain wall mobility in nanowires: Transverse versus vortex walls, Physical Review B 69, 064401 (2004).
18. A. Belabbes, G. Bihlmayer, S. Bluegel, and A. Manchon, Oxygen-enabled control of Dzyaloshinskii-Moriya interaction in ultra-thin magnetic films, Science Reports 6, 24634 (2016).
19. H. Yang, O. Boulle, V. Cros, A. Fert and M. Chshiev, Controlling Dzyaloshinskii–Moriya interaction via chirality dependent layer stacking, insulator capping and electric field, Scientific Reports Vol, 8, issue 1, PP 12356, (2018).
20. L. Herrera Diez, Y. T. Liu, D. A. Gilbert, M. Belmeguenai, J. Vogel, S. Pizzini, E. Martinez, A. Lamperti, J. B. Mohammedi, A. Laborieux, Y. Roussign\'e, A. J. Grutter, E. Arenholtz, P. Quarterman, B. Maranville, S. Ono, M. Hadri, El. Salah El, R. Tolley, E. E. Fullerton, L. Sanchez-Tejerina, A. Stashkevich, S. M. Chèrif, A. D. Kent, D. Querlioz, J. Langer, B. Ocker and D. Ravelosona, Nonvolatile Ionic Modification of the Dzyaloshinskii-Moriya Interaction, Phys. Rev. Appl., 12 034005 (2019).
21. H. T. Nembach, E. Jué, E. R. Evarts and J. M. Shaw, Correlation between the Dzyaloshinskii-Moriya interaction and the orbital angular momentum at an oxide/ ferromagnet interface, Physical Review A 101, 020409 (2020).
22. H. T. Nembach, J. M. Shaw, M. Weiler, E. Jué and T. J. Silva, Linear relation between Heisenberg exchange and interfacial Dzyaloshinskii -Moriya interaction in metal films, Nat. Phys. Lett, 3418, (2015).
23. C. Vaz, J. Bland and G. Lauhoff, Magnetism in ultrathin film structures, Rep. Prog. Phys. 71, 056501 (2008).
24. J. M. Shaw, H. T. Nembach, M. Weiler, T. J. Silva, M. Schoen, J. Z. Sun and D. C. Worledge, Perpendicular Magnetic Anisotropy and Easy Cone State in $Ta/Co_{60}Fe_{20}B_{20}/MgO$, IEEE Magn. Lett., Volume 6 (2015).

25. J. M. Shaw, H. T. Nembach and T. J. Silva, Measurement of orbital symmetry and strain in $Co_{90}Fe_{10}$/Ni multilayers and alloys: Origin of perpendicular anisotropy, Physical Review B 87, 054416 (2013).
26. H. T. Nembach, T. J. Silva, J. M. Shaw, M. L. Schneider, M. J. Carey, S. Maat, and J. R. Childress, Perpendicular ferromagnetic resonance measurements of damping and Landè g- factor in sputtered $(Co_2Mn)_{1-x}Ge_x$ thin films, Physical review B 84, 054424 (2011).
27. C. W. Cheng, W. Feng, G. Chern, C. M. Lee and Te-ho Wu, Effect of cap layer thickness on the perpendicular magnetic anisotropy in top MgO/CoFeB/Ta structures. J. of Appl. Phys., Vol 110, 033916 (2011). https://doi.org/10.1063/1.3621353
28. M. Kowalewski, H. Butler, N. Moghadam, M. Stocks, G and C. Schulthess, T and Song, Kyu Jeong and R. Thompson, J and Arrott, A and Zhu, T and Drewes, J and R. Katti, R and T. McClure, M and Escorcia, O, The effect of Ta on the magnetic thickness of permalloy ($Ni_{81}Fe_{19}$) films. Journal of Applied Physics, volume 87, pages 5732-5734 (2000), doi = {10.1063/1.372504}
29. S. H. Shen, D. S. Lee, C. W. Cheng, W. J. Chan and G. Chern, The Correlation Between Magnetic Dead Layer and Perpendicular Magnetic Anisotropy in MgO/CoFeB/Ta Top Structure, IEEE Transactions on Magnetics, Volume 55, (2019), doi = {10.1109/TMAG.2018.2876371}
30. A. Manchon, C. Ducruet, L. Lombard, S. Auffret,B. Rodmacq, B. Dieny, S. Pizzini, J. Vogel, V. Uhl´ıř,M. Hochstrasser, and G. Panaccione, Analysis of oxygen induced anisotropy crossover in Pt/Co/MOx trilayers, J. Appl. Phys.104,043914 (2008).
31. S. Monso, B. Rodmacq, S. Auffret, G. Casali, F. Fettar,B. Gilles, B. Dieny, and P. Boyer, Crossover from in-plane to perpendicular anisotropy in Pt/CoFe/AlOx sandwiches as a function of Al oxidation: A very accurate control of the oxidation tunnel barriers, Applied Physics Letters 80,4157 (2002).
32. B. Rodmacq, S. Auffret, B. Dieny, S. Monso, and P. Boyer, Crossover from in-plane to perpendicular anisotropy in magnetic tunnel junctions as a function of the barrier degree of oxidation, J. Appl. Phys. 93, 7513 (2003).
33. H. X. Yang, M. Chshiev, B. Dieny, J. H. Lee, A. Manchon, and K. H. Shin, First-principles investigation of the very large perpendicular magnetic anisotropy at Fe|MgO and Co|MgO interfaces, Phys. Rev. B 84, 054401 – Published 1 August 2011

34. D. de Souza Chaves, F. Ajejas, V. Krizakova, J. Vogel, and Stefania Pizzini, Dependence of Dzyaloshinskii-Moriya interaction on the oxygen coverage in Pt/Co/MOx trilayers, arXiv:1708.08516v1 [cond-mat. mtrl-sci] 28 Aug 2017
35. T. Devolder, S. Couet, J. Swerts, G. S. Kar, Gilbert damping of high anisotropy Co/Pt multilayers, J. Phys. D:Appl. Phys. 51 135002 (2018).
36. O. Mosendz, J. E. Pearson, F. Y. Fradin, S. D. Bader, and A. Hoffmann, Suppression of spin-pumping by a MgO tunnel-barrier, Applied Physics Letters, 96, 022502 (2010).
37. Duck-Ho Kim, Hong-Hyoun Kim, and Chun-Yeol You, Suppression of the spin pumping in Pd/Ni81Fe19 bilayers with nano-oxide layer, Appl. Phys. Lett. **99**, 072502 (2011).
38. Sang-Il Kim, Min-Su Seo, Jung-Hye Seo, Hyung Joong Yun, Jouhahn Lee, Yeon Suk Choi, Seung-young Park, Abnormal spin-pumping effect at Pt/NiFe interface by an oxidation of ferromagnet, Current Applied Physics, Volume 14, Issue 12, December 2014, Pages 1743-1747.
39. B. L. Zink, M. Manno, L. O'Brien, J. Lotze, M. Weiler, D. Bassett, S. J. Mason, S. T. B. Goennenwein, M. Johnson, and C. Leighton, Efficient spin transport through native oxides of nickel and permalloy with platinum and gold overlayers, Phys. Rev. B 93, 184401 (2016).
40. C. T. Boone, H. T. Nembach, J. M. Shaw and T. J. Silva, Spin transport parameters in metallic multilayers determined by ferromagnetic resonance measurements of spin-pumping, Journal of Applied Physics 113, 153906 (2013).
41. P. Jadaun, L. F. Register, and S. K Banerjee, The microscopic origin of DMI in magnetic bilayers and prediction of giant DMI in new bilayers, arXiv:1903.09345v3 [cond-mat.mtrl-sci] 30 Sep 2019.
42. A. Belabbes, and G. Bihlmayer, and F. Bechstedt, and S. Blügel, and A. Manchon, Hund's Rule-Driven Dzyaloshinskii-Moriya Interaction at 3d-5d Interfaces. Physical Review Letters., 117, issue 24, pages 247202, (2016).
43. V. Kashid, T. Schena, B. Zimmermann, Y. Mokrousov, S. Blugel, V. Shah and H. G. Salunke, Dzyaloshinskii-Moriya interaction and chiral magnetism in 3d–5d zigzag chains: Tight-binding model and ab initio calculations. Phys. Rev. B 90, 054412 (2014).

44. S. Bornemann, O. Šipr, S. Mankovsky, S. Polesya, J. B. Staunton, W. Wurth, H. Ebert, J. Minár, Trends in the magnetic properties of Fe, Co, and Ni clusters and monolayers on Ir(111), Pt(111), and Au(111). Phys. Rev. B 86, 104436 (2012).
45. S. Tacchi, R. E. Troncoso, M. Ahlberg, G. Gubbiotti, M. Madami, J. Ákerman, and P. Landeros, Interfacial Dzyaloshinskii-Moriya Interaction in Pt/CoFeB Films: Effect of the Heavy-Metal Thickness, Phys. Rev. Lett. 118, 147201 (2017).
46. A. K. Chaurasiya, S. Choudhury, J. Sinha, and A. Barman, Dependence of Interfacial Dzyaloshinskii-Moriya Interaction on Layer Thicknesses in Ta/Co-Fe-B/TaOx Heterostructures from Brillouin Light Scattering, Phys. Rev. Appl. 9, 014008 (2018).
47. T. Moriya, Anisotropic super-exchange interaction and weak ferromagnetism. Phys. Rev. 120, 91–98 (1960).